Article

The (Building) Stones of Venice under Threat: A Study about Their Deterioration between Climate Change and Land Subsidence

Gloria Zaccariello [ID], Elena Tesser [ID], Rebecca Piovesan [ID] and Fabrizio Antonelli *[ID]

LAMA—Laboratory for Analysing Materials of Ancient Origin, Iuav University of Venice, San Polo 2468, 30125 Venezia, Italy; gzaccariello@iuav.it (G.Z.); etesser@iuav.it (E.T.); rpiovesan@iuav.it (R.P.)
* Correspondence: fabrizio.antonelli@iuav.it

Abstract: Cultural heritage assets face significant threats from climate change and land subsidence, leading to extensive social, economic, and environmental losses, and damage to artistic and monumental heritage in Italian coastal cities. In particular, addressing these challenges in the Venetian context necessitates the development of an adaptation plan for the lagoon area and the identification of targeted intervention strategies to preserve cultural and territorial heritage. To address these objectives, a systematic study was conducted to investigate the deterioration patterns exhibited by the most representative lithologies used in Venetian buildings. Thirty samples of five carbonate stone varieties subjected to natural aging were monitored in six different areas of Venice's historic center and on Torcello Island, selected based on altimetry relative to tidal zero and exposure to environmental forces. An integrated multi-analytical approach was employed to identify and map macro- and micro-morphologies of stone surfaces related to chemical weathering and physical decay. Stones underwent evaluation during nine monitoring periods using various tests (ultrasound P-wave velocity and colorimetric measures) and analyses (µX-Ray Fluorescence, X-ray powder diffraction, stereomicroscope observations, and recognition of biological patinas). Data processing aimed to elucidate how microclimate and intrinsic stone features influence the occurrence and progression of deterioration phenomena. From the experimental findings, a Stone Deterioration Index and Intervention Procedures (*SDIi*) were proposed to estimate deterioration rates and assess the need for targeted intervention through conservative actions.

Keywords: cultural heritage; climate change; land subsidence; eustatism; high tide; Venice; stone materials; carbonate rocks; stone deterioration; weathering

1. Introduction

Tangible cultural heritage suffers from detrimental effects exacerbated by climate breakdown, due to shifts in temperatures and weather patterns that affect, among others, precipitation, atmospheric moisture and wind intensity. Direct consequences of climate crisis are the sea flooding and sea level rise. For this reason, the vulnerability of artistic, architectural and monumental heritage in lagoonal and marine environments is increasingly threatened. In this context, an immediate intervention for the safeguarding of the city of Venice has become a real emergency to protect monuments and historical buildings from climate change impacts [1,2].

From the beginning of the last century to the 1970s, the eustatic rise in Venice was 9 cm, as reported by the Forecast and Tide Centre of the City of Venice. In addition, Venice is hit by the subsidence phenomenon. Due to natural and anthropogenic damages, the sinking of the island is primarily caused by the drawing of groundwater that has been intensive in the past, especially in the industrial area of Marghera. From 1950 to 1970, the lowering of the soil was approximately 12 cm in the areas surrounding Venice. Eustatism and subsidence have contributed to the change in mean sea level (m.s.l.), which currently

is about 32 cm (average of the last 15 years) higher than it was in 1897. The maximum increase occurred from 1930 to 1970 because of the combined effects of sea level rise and lowering of the soil. After that period, until 2008, the main sea level seems to attain a fairly constant value. Then, the m.s.l. shows again an increased trend [2,3].

Subsidence and eustatism also contribute to the so-called *acqua alta* phenomenon (literally high water), the exceptional tide peaks that periodically occur in the Adriatic Sea reaching their maximum in the Venetian lagoon. This natural phenomenon generally takes place in autumn and springtime due to the combination of astronomical tide, strong south wind and seiche [1]. High water levels are measured on the tidal zero at *Punta della Salute* (located near the Salute Church, in front of St. Mark Square) and 97% of the town is at +100 cm. Conventionally, a sea level higher than 80 cm above the local datum of *Punta della Salute* is considered as high tide in Venice. When the tide exceeds 100 cm (5% of public land flooded), the phenomenon begins to affect large sections of pedestrian areas. About 12% of the city is affected by flooding at +110 cm and about 59% of the city is flooded at +140 cm. Moreover, the synergic effect of subsidence and eustatism have influenced the high tide frequency in the last 60 years, as reported by the Forecast and Tide Centre of the City of Venice. Since 2010, the situation has become dramatic as the number of high-tide events exponentially increased. Particularly, twenty-six high tides ($\geq$110 cm) were recorded between November and December 2019. On 12 November 2019, the city was hit by the highest tide in more than 50 years, with an intense high water peaked at +187 cm. Until 1950, there was an almost stationary trend of high tides for about eighty years as shown in the graph in Figure 1. In recent decades, as reported in the historical archive published on the website of the Forecast and Tides Centre, the frequency has greatly increased, reaching 52 events during the years 2000–2009 and 118 events from 2010 to nowadays (Figure 1c).
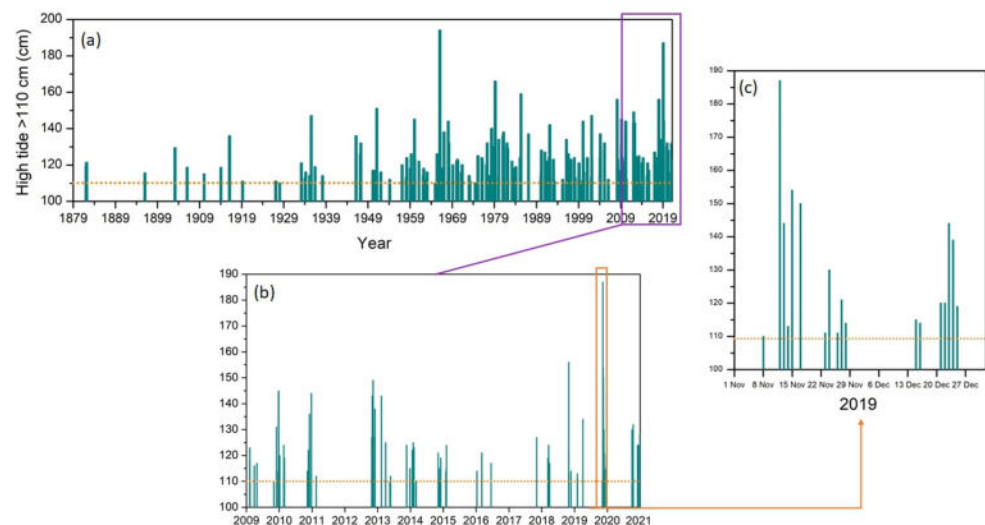

Figure 1. Yearly distribution of high tides $\geq$ 110 cm recorded in Venice, from 1872 to 2021 (**a**). Image (**b**) focuses on 2009–2021 period, whereas image (**c**) only on 2019.

The repeated flood of brackish lagoon water into the city represents severe problems not only because the overflowing of the canals leads to the flooding of the pedestrian walkways, but also because the interaction between water and the buildings induces serious deterioration effects on architectural heritage (i.e., mechanical damages, cracks, erosions, efflorescences, chromatic alterations and biological colonizations) [2–7]. Aiming at abating these issues and protecting the city and the Venetian lagoon from flooding, the MOSE (*MOdulo Sperimentale Elettromeccanico*/Experimental Electromechanical Module) project was proposed in 1980. The project is an integrated system consisting of rows of mobile gates able to isolate the Venetian lagoon temporarily from the Adriatic Sea during high tides. The operating procedure dictates that the gates are raised for tides $\geq$ 110 cm [2]. The authorities have established this value as the optimum height for the current sea levels.

The activation of the MOSE system from 20th October 2021 is underlined in the graph reporting the theoretical cases of high tide as calculated from the tidal forecasts.
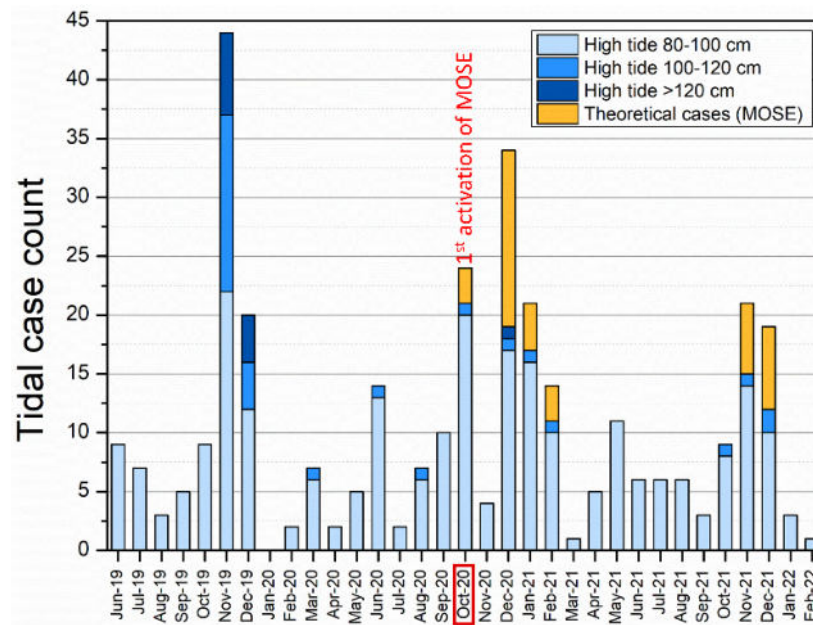

Figure 2. Tidal case count, considering different ranges of high tide (80–100 cm; 100–120 cm; >120 cm), from June 2019 to February 2022. The activation of the MOSE system from 20 October 2021 is underlined reporting the theoretical cases of high tide as calculated from the tidal forecasts.

In this context, the present research, which is part of the project "*Venezia 2021- Programma di ricerca scientifica per una laguna regolata*" (a scientific activity performed in the Research Programme Venezia2021, with the contribution of the *Provveditorato* for the Public Works of Veneto, Trentino Alto Adige and Friuli Venezia Giulia, provided through the concessionary of State *Consorzio Venezia Nuova* and coordinated by *CORILA*), aims to better understand the effects of the environmental forcings on the deterioration of the stone materials used in the Venetian historical buildings and to support the development of strategies for their preservation. For this purpose, six different building sites in Venice and *Torcello* Island were selected to place five of the most common carbonate building stones, with different porosity and texture, used in the Venetian architectural surfaces [7–9]. These sites were chosen according to both the different altimetry with respect to the tidal zero and the different exposure to environmental forcings. The ability to detect chemical weathering effects and track the decay patterns exhibited by stone specimens enabled to assess the impact of high tides on building surfaces and estimate the timing of deterioration phenomena development through a comprehensive multi-analytical approach [10]. To advance the implementation of novel strategies and protocols aimed at preserving and safeguarding the architectonic-monumental heritage of Venice, a forecasting model and a possible deterioration-intervention index specifically tailored to stone materials and based on non-destructive tests carried out with portable instruments were developed. These tools lend support to the notion of long-term decay prediction.

2. Experimental Section

2.1. Materials

The selection of the stone subjected to natural ageing was made considering the most common lithotypes in the historical Venetian building. Five different carbonate stone varieties (four limestones and one pure isotropic marble) were chosen, i.e., *Ammonitico rosso from Verona*, *Istrian Stone*, *Vicenza Soft Stone*, *Aurisina Fiorita Stone* (a variety with a grey background and macroscopic fossil patterns), and *White Carrara Marble*. The samples, each measuring $5 \times 5 \times 2$ cm, were placed in a polymeric sample holder (Figure 3). Five pairs of sample holders were placed in the selected areas of the Venice historic centre and one on *Torcello* Island. The sites were: (1) *Ca' Foscari* (Dorsoduro district); (2) *San Giobbe* economic campus of *Ca' Foscari* University (Cannaregio district); (3) *Palazzo Badoer* (San Polo district); (4) *Ca' Tron* (Santa Croce district); (5) *Palazzo Malipiero* (San Marco district); (6) the remains of the small church dedicated to St. Mark on *Torcello* Island. Figure 4 reports the Venice map and the selected sites. In each building, two sample holders were positioned directly on the original brick walls at two different altimetry with respect to the mareographic zero. The first sample holder of each pair was placed in correspondence to the ground level (referred to as "position 1—P1"), while the second one just over 110 cm (referred to as "position 2—P2") since it is considered as the tidal reference level for the activation of the MOSE mobile bulkheads.

The specimens exposed to natural ageing were monitored every three months, from June 2019 up to February 2022, for nine monitoring sessions.

The specimens were labeled as S-Ly_t_x, where:

- S was referred to the site: F (*Ca' Foscari*), G (*San Giobbe* campus), B (*Palazzo Badoer*), T (*Ca' Tron*), M (*Palazzo Malipiero*) and Tor (*Torcello* Island);
- L was referred to the lithology: C (White Carrara marble), V (Vicenza Soft Stone), I (Istrian Stone), R (=Ammonitico Rosso from Verona), A (Aurisina Fiorita Stone);
- y was referred to the position with respect to the altimetry: 1 (position 1—ground level), 2 (position 2– $\geq$ 110 cm);
- t_x was referred to time zero or to the number of the monitoring with values of x from 0 to 9.
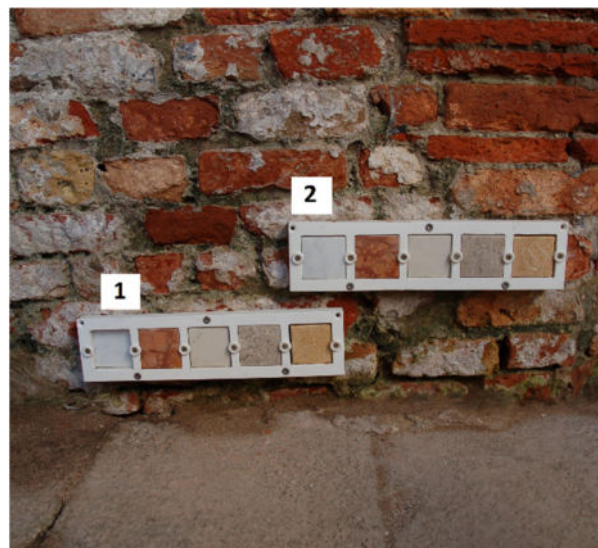

Figure 3. Example of how the specimens were placed in a sample holder and fixed on the original masonry. The number 1 refers to the ground level (P1) and the number 2 to altimetry $\geq$ 110 cm (P2).
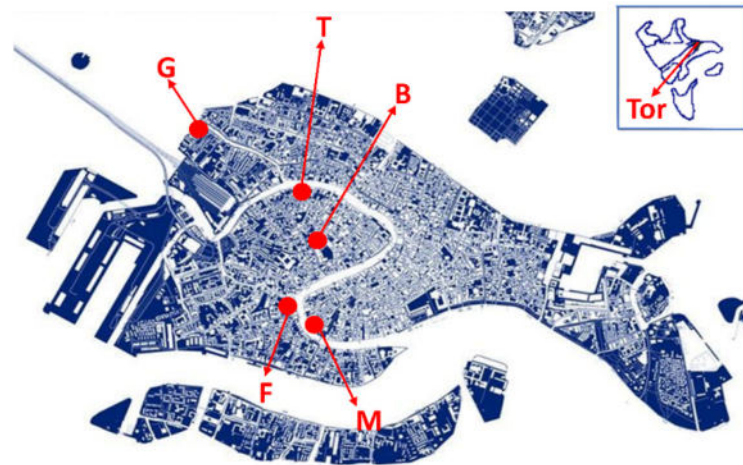
Figure 4. Venice map and samples locations: *Ca' Foscari* (F); *San Giobbe* campus (G); *Palazzo Badoer* (B); *Ca' Tron* (T); *Palazzo Malipiero* (M); the remains of the small church dedicated to St. Mark on *Torcello* Island (Tor).

2.2. Experiments

Before the outdoor exposure, diagnostic investigations useful for the mineralogical-petrographic, chemical-physical and morphological characterization were carried out on each stone specimen. These data represent a benchmark (at time zero = t_0) used as a reference for comparing all the data collected during the subsequent monitoring steps. The monitoring was planned to allow a systematic characterization of the state of conservation of the samples on a quarterly basis.

Before each monitoring analysis, the samples were placed in an oven at 50 °C for 24 h and then in a dryer for 3 h.

To study the nature of any deposits and spots on the surface of samples, X-ray Fluorescence (XRF) spectra were collected using a Bruker M4 Tornado μ-XRF apparatus. For elemental mapping, a current of 200 μA and a voltage of 50 kV were used. The chamber pressure was set at 20 mbar. The elemental maps were collected over an area of 1 cm^2 with a step size of 20 μm. The μ-XRF analyses were performed without any further preparation of the samples.

Mineralogical analyses were performed on fine-grained powder of efflorescence samples (obtained with a hand mortar) by X-ray powder diffraction (XRPD) using a Panalytical Empyrean diffractometer, operating at 40 kV and 40 mA, in Bragg-Brentano reflection geometry and equipped with CuKα radiation and an X'Celerator detector. Qualitative analysis of diffraction data was carried out with X'Pert HighScore Plus® 3.0b (3.0.2) software (PANalytical) and the PDF-2 database.

Colorimetric analyses were executed aiming at evaluating chromatic variations of the samples during the outdoor exposure. The color measurements were made in the *CIE L***a***b** color space, where L^* is the lightness (positive and negative values), while a^* and b^* are the chromaticity coordinates (the red-green and the yellow-blue direction, respectively).

The total color variation (ΔE^*) was calculated as follows:

$$\Delta E^* = \sqrt{\Delta L^{*2} + \Delta a^{*2} + \Delta b^{*2}} \tag{1}$$

According to the EN 15886:2010 standard, color data were acquired with a CM-2600d Konica Minolta portable spectrophotometer with a D65 illuminant and 10° standard observer [11]. This instrument has a 5 mm diameter measurement area and it was set to quantify the potential specular component included (SCI) color variations. To obtain reliable and reproducible measurements, an average of five points with three scans each was considered for each specimen [12]. Color variation values were considered acceptable

when $\Delta E^* < 5$, critical for $\Delta E^* > 5$ values since an observer can notice two different colors, and drastic when $\Delta E^* > 12$ [13,14].

The investigations of eventual superficial patina development of organic and/or inorganic nature were carried out through morphological observations using a Leica F12I stereomicroscope.

The recognition of biological deterioration was made through the observation of freshly prepared slides through a Leitz LABORLUX 12 POL S microscope (UNI 10923: 2001) [15].

In order to investigate the compactness of the specimens and possible alterations of the inner porosity over time, ultrasound speed was monitored using a Matest C369N equipped with 55 kHz probes. Electrodes were positioned in opposite positions, at the bottom and top of the sample, maintaining a consistent central position for all measurements [16]. An average of three tests were performed for each specimen during every monitoring. Due to the specimens dimensions ($5 \times 2 \times 2$ cm edge) and the exposure position, the measures were performed only orthogonally to the exposed surfaces.

A Flir E8xt thermographic camera was used to detect subtle temperature differences and patterns that reveal the existence of water on the walls in which the samples were placed.

3. Results and Discussions

3.1. Natural Ageing Results

The variation of the physical properties, texture, mineralogical and chemical compositions of the rocks after weathering was directly linked to the intrinsic properties of each lithotype and the environmental forcings. All the deterioration effects and morphologies observed on the samples exposed in the different sites are described below. The altimetry of each area considered and the samples high referred to positions 1 and 2 are reported in Table 1, while the description of the outdoor conditions (light exposure, wind, marine aerosols, rain and wave motion) to which the specimens were subject in each site and each position are summarized in Table 2.

Table 1. Altimetry of each site (referred to the area/district) and height of the samples in positions 1 and 2. Data from Insula Spa.

| Altimetry | Sites | | | | | |
	Ca' Foscari **(F)**	*San Giobbe* **(G)**	*Palazzo Badoer* **(B)**	*Ca' Tron* **(T)**	*Palazzo Malipiero* **(M)**	*Torcello* **Island (Tor)**
Area	135 cm	120 cm	101 cm	98 cm	110 cm	/
Position 1	108 cm	120 cm	105 cm	100 cm	100 cm	110 cm
Position 2	145 cm	145 cm	110 cm	125 cm	120 cm	125 cm

Table 2. Description of the environmental conditions to which the specimens were subject in each site and each position (referred to the area/district). P1 and P2 are referred to the position of the samples with respect to the ground floor. ✓ = subjected to; ✗ = not subjected.

| Site | Environmental Conditions | | | | | |
	Outdoor/Indoor	Wind Directions	Direct Rain	Direct Light	Channel	Wave Motion
Ca' Foscari **(F)**	Outdoor	P1: from South-West to West P2: from South-West to North/North-West	✓	✓	✓	✓
San Giobbe **campus (G)**	Outdoor	P1/P2: to South-West and North/North-East	✓	✓	✓	✗

Table 2. *Cont.*

Site	Environmental Conditions					
	Outdoor/Indoor	Wind Directions	Direct Rain	Direct Light	Channel	Wave Motion
Palazzo Badoer **(B)**	Outdoor	P1/P2: -East	✗		✗	✗
Ca' Tron **(T)**	Indoor	✗	✗	✗	✓	✗
Palazzo Malipiero **(M)**	Indoor	✗	✗	✗	✓	✓
Torcello **Island (Tor)**	Outdoor	P1/P2: from South-East to South-West	✓	✓	✗	✗

A.   Chromatic alterations

All the lithologies showed chromatic variations depending on exposure and their intrinsic properties (Figure S1a–e).

Most of the specimens in *Aurisina Fiorita Stone* darkened over time, except those (i) at *Palazzo Badoer* located in a sheltered position, (ii) indoors at *Ca' Tron* far away from pollutants and weathering and (iii) at *San Giobbe* campus facing the lagoon and subjected to winds exposure and washout. The specimens in *Aurisina Fiorita Stone* showed the most significant chromatic variations at *Palazzo Malipiero*, because of the constant wave motion and high tides, which induce the development of algae and cyanobacteria.

White Carrara Marble displayed two types of chromatic alterations. In most of the sites, a tendency to whiten was detected. Especially in *San Giobbe* campus, the specimens denote a drastic chromatic change from zero time ($\Delta E^* > 12$) here in both positions. Furthermore, *White Carrara Marble* specimens showed a superficial yellowing visible to the naked eye over time (see Figure S2). Reflectance curves from colorimetric analysis confirmed this color change, as shown in Figure 5. The reason for this decay phenomenon is the leaching of iron from pyrite (FeS_2)—an accessory mineral which is very common in the Carrara marble—and the subsequent formation of iron hydroxides [i.e., limonite $FeO(OH) \cdot nH_2O$] [17]. Water vehicles iron to the marble surface, where it precipitates as colored iron hydroxide and produces staining [7,18,19]. Iron-bearing minerals, including iron sulphides among others, are present to various degrees in marble, dispersed into the carbonate mass or concentrated along veins.

Istrian Stone specimens did not show any significant chromatic variations, except those located at *Palazzo Malipiero* and *Palazzo Badoer* (position 1). In the first case, the color change was related to the development of biological species on the specimen surface (as described in section D). In the latter case, a darkening of the surface occurred probably linked to atmospheric particulate deposition in a shelter location not exposed to driving rain and washout phenomena.

Ammonitico Rosso from Verona mitigated the original tones slightly. Only the specimens placed at *Palazzo Malipiero* showed an outstanding color change due to biodeteriogens.

Finally, all the specimens in *Vicenza Soft Stone* reported a noticeable superficial darkening even at a macroscopic level. The greatest porosity of this lithotype compared to the others [8] as well as the greater roughness of its surface (being a non-polishable stone) facilitated the deposition of (i) atmospheric particulate (i.e., *Palazzo Badoer*) and/or (ii) spores, with the consequent growth of biodeteriogens (such as in *Palazzo Malipiero*), as well as (iii) a great water capillary absorption capacity and the consequent efflorescence appearance (particularly marked in *Ca' Tron* samples). All these deterioration morphologies necessarily lead to a chromatic variation of the specimens.
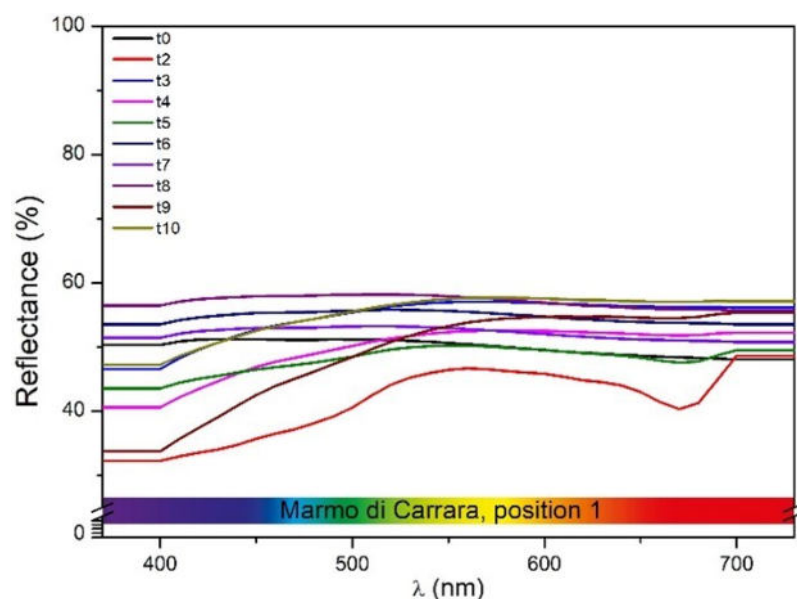
Figure 5. Reflectance curves of *White Carrara Marble* specimen located at *Palazzo Malipiero* (P1) from t_0 to t_{10} (from June 2019 to February 2022).

B. Efflorescence

The marine aerosols and periodic high waters lead to salt crystallization on the surface of the specimens. The determination of the distribution of the efflorescences and the quantitative estimation of the salts present were conducted through microscopic observations and μXRF elemental analysis, respectively.

XRPD and ionic chromatography techniques—which imply the mechanical sampling of superficial powder from specimens, inducing possible modification of the exposed surfaces and potential loss of relevant information for the continuous monitoring of weathering process—were normally avoided for the periodic evaluation of conservation states. However, the presence of abundant salt efflorescences observed on specimens located in *Palazzo Malipiero* and *Ca' Foscari* at t3 allowed safe sampling and XRPD analyses. Their mineralogical composition resulted based on halite (NaCl).

All chemical analyses performed by μXRF confirmed the presence of chlorine and sodium on the surface of the samples during time; these elements are not ascribable to the chemical composition of the stones. Table 3 shows the percentage values (maximum atomic concentration) of chlorine distribution referred to sodium chloride for each exposed specimen.

Table 3. Maximum atomic concentrations of chlorine detected by μXRF analysis.

Lithotype	Position	*Palazzo Badoer*	*Ca' Tron*	*San Giobbe*	*Ca' Foscari*	*Palazzo Malipiero*	*Torcello Island*
White Carrara Marble	1.	2%	12%	2%	5%	4%	1%
	2.	2%	9%	2%	1%	4%	1%
Istrian Stone	1.	3%	8%	1%	6%	4%	1%
	2.	2%	15%	1%	/	7%	/
Aurisina Fiorita Stone	1.	37%	34%	10%	3%	15%	10%
	2.	29%	23%	8%	26%	38%	5%
Ammonitico rosso from Verona	1.	3%	22%	1%	3%	4%	1%
	2.	5%	15%	2%	/	4%	1%
Vicenza Soft Stone	1.	32%	59%	30%	43%	55%	32%
	2.	29%	47%	36%	45%	38%	24%

The collected data led to the conclusion that *Ca' Tron* is the site where all the lithotypes were significantly affected by the formation of halite crystals, as indicated by the very high concentrations of chlorine and verified by the XRPD analysis performed on t_3. This was especially so for the substrates in *Aurisina Fiorita Stone* and *Vicenza Soft Stone* (P1 and P2). The environment in which these specimens were placed is closed, without ventilation, and not equipped with a heating/refrigeration or dehumidification system, near to a water gate facing the canal. Although the area is far from wave motion and direct marine aerosol, it is strongly affected by capillary rising phenomenon, compromising the conservation of the lithotypes, as shown in Figure 6. Thermal imaging confirmed the conditions to which the samples were subjected, detecting moisture damage located behind interior walls (Figure 7).
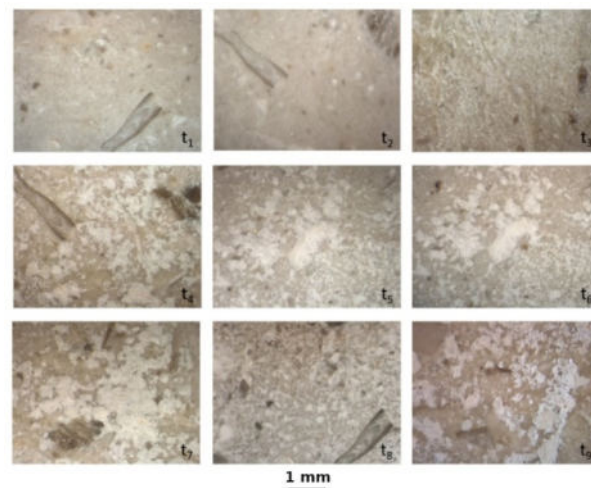

Figure 6. Stereographs of the specimen of *Aurisina Fiorita Stone* exposed at *Ca' Tron* (P2) from September 2019 to February 2022 (from t_1 to t_9).
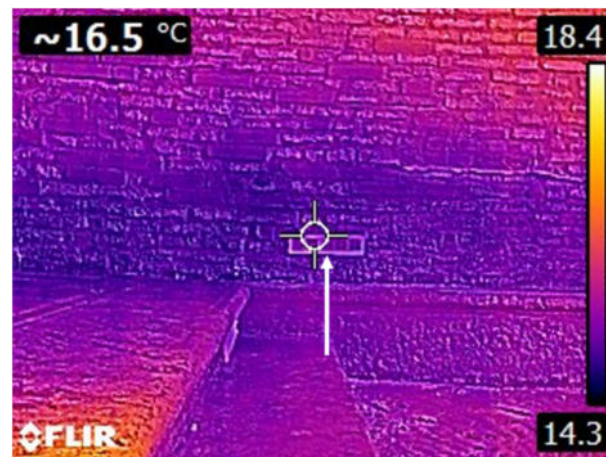

Figure 7. Thermographic analysis of the samples located in P2 exhibited at *Palazzo Malipiero*.

In all the other sites, only the specimens in *Aurisina Fiorita Stone* and *Vicenza Soft Stone* reported a significant crystallization of salts, probably due to the greater porosity of these lithotypes. The textural characteristics and the low porosity (often less than 1% by volume) of *White Carrara Marble*, *Istrian Stone* and, with a lesser extent, *Ammonitico Rosso* from Verona, partially limit water absorption and counteract salts migration and crystallization [4]. Although efflorescences appeared in the samples placed near ground level (P1), the most relevant degradation phenomena were observed in the samples placed at $\geq$110 cm (P2), as the consequence of rising dumps and wet-dry or moisty-dry cycles [20–22].

C. Subflorescence

The specimens in *Ammonitico Rosso from Verona* exposed at *Ca' Tron*, *San Giobbe* campus, *Palazzo Malipiero* and *Torcello* island showed the formation of small areas, orange in colour and swollen, increasing over time, as observed with microscope. This damage is related to the crystallization of salts inside the pores of the stone as cryptoflorescences, with the consequent development of crystallisation pressure. This phenomenon can lead to severe deterioration of the stone, due to the breaking of the surface and the loss of material over time, especially along the clayey layers that characterize this kind of rock [20]. Indeed, lay minerals have the capacity to absorb large quantities of water by expanding their network. When the evaporation rate of water containing dissolved salts is greater than the capillary rise rate, the salts tend to crystallize before the solution reaches the exposed surface, giving rise to subflorescence. Over time, the crystallization pressure exerted during the process can cause lifting and detachment. Figure 8 shows an example of subflorescence developed in *Ammonitico Rosso* from Verona specimen exposed in *Palazzo Malipiero* (P1) over time.
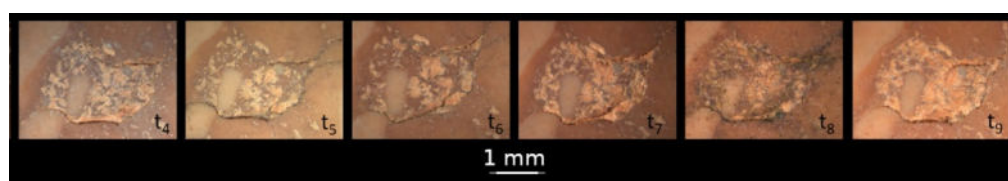

Figure 8. Stereographs of subflorescence developed over time in *Ammonitico Rosso* specimen exposed at *Palazzo Malipiero* (P1).

D. Sulphation

The elemental surface analysis also revealed significant levels of sulphur (Table 4) strongly linked to the presence of this pollutant in the Venetian atmosphere. As it is well known, the presence of sulphur on carbonate matrices can induce the development of gypsum, through the chemical reaction of sulphation [23,24]. Quantitative chemical analysis revealed a variable distribution of this element depending on the lithotype and the exposure.

Table 4. Maximum atomic concentrations of sulphur detected by µXRF analysis.

Lithotype	Position	*Palazzo Badoer*	*Ca' Tron*	*San Giobbe*	*Ca' Foscari*	*Palazzo Malipiero*	*Torcello* **Island**
White Carrara Marble	1.	/	/	/	/	/	/
	2.	4%	/	/	2%	/	/
Istrian Stone	1.	/	/	/	3%	/	/
	2.	/	/	/	/	/	/
Aurisina Fiorita Stone	1.	17%	13%	4%	7%	/	2%
	2.	6%	5%	8%	2%	/	/
Ammonitico rosso from Verona	1.	/	/	/	/	/	/
	2.	5%	/	/	/	/	/
Vicenza Soft Stone	1.	15%	34%	23%	10%	10%	4%
	2.	8%	/	5%	3%	2%	2%

The lithotypes that suffered the most from the reaction with sulphur are *Aurisina Fiorita Stone* and *Vicenza Soft Stone* (P1). The stones exposed in Venice showed a more marked presence of sulphur than those located on *Torcello* Island. In particular, the highest concentrations were recorded at *Palazzo Badoer*, *Ca' Tron* and *San Giobbe* campus with no correlation to the characteristics of each site (sheltered, closed or facing the canal). The cause lies, most probably, in the greater abundance of pollutants connected to vehicular traffic, diffused not only in the atmosphere but also in the water and which, through the action

of aerosols and the phenomenon of capillary rise, react with the carbonate masses. In the case of *San Giobbe* campus, the direct contact with rain or acid mist and the direct exposure to industrial emissions from *Porto Marghera*, rich in nitrogen oxides and sulphur (NO_x and SO_2), carry out a potentially more aggressive effect on exposed stone surfaces. The sulphur quantity recorded drastically decreased during lockdown period due to COVID-19 pandemic emergency [25].

E.   Superficial concretions

As exemplified in Figure 9, superficial limestone incrustations were formed in some specimens of *Istrian Stone*. In particular, the growth of these concretions took place in the specimens exposed at *San Giobbe* campus, *Ca' Foscari* (only P1), *Ca' Tron* and *Torcello* Island (only P2). The deposition of secondary calcite in the concrete state is a direct consequence of the environmental conditions to which these specimens were subjected. Indeed, the continuous occurrence of humidity and drying cycles (wet and dry) leads to the dissolution of the primary calcite and the subsequent re-precipitation of calcium carbonate in the surface pores of the stone. The deposit and growth of secondary calcite crystals, much more fragile than those of primary origin, facilitate micro-cracks and decohesions, resulting in loss of material and increasing superficial porosity [26].
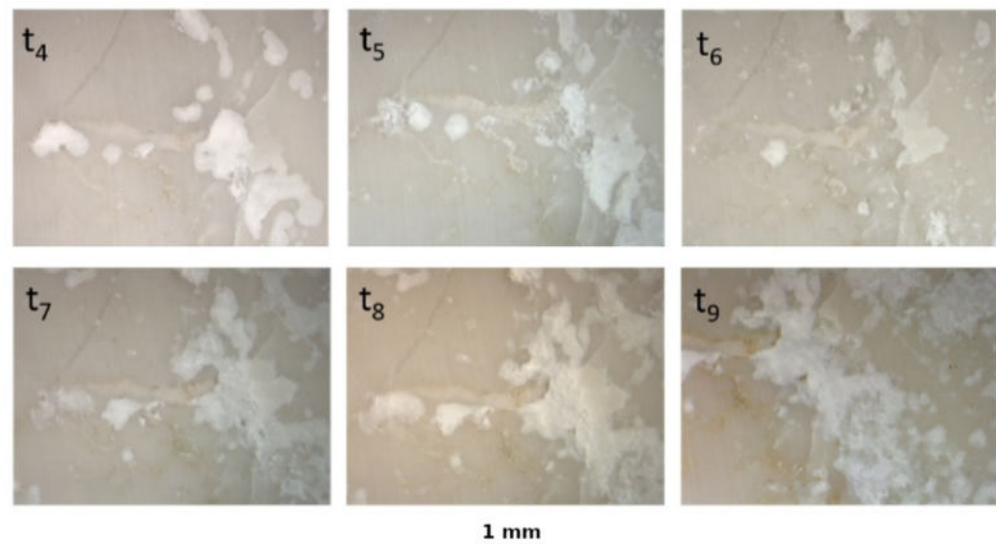

Figure 9. Stereographs of the growth of superficial calcareous concretions of *Istrian Stone* specimen exposed at *Ca' Tron* (P2).

F.   Loss of material

The specimen in *Ammonitico Rosso* from Verona placed in P2 at *Palazzo Malipiero* showed a consistent detachment of material in correspondence with the stylolithic joints, which are characterized by the presence of expanding clay minerals (smectites) [27,28]. Likewise, the *Vicenza Soft Stone* specimen, exposed in the same location, underwent an important detachment along a structural discontinuity represented by some bioclasts [29]. Consequently, the continuous expansion/contraction process and the saline crystallisation, particularly relevant for direct exposure to the canal, resulted in the physical decay of the samples, as showed in Figure 10.
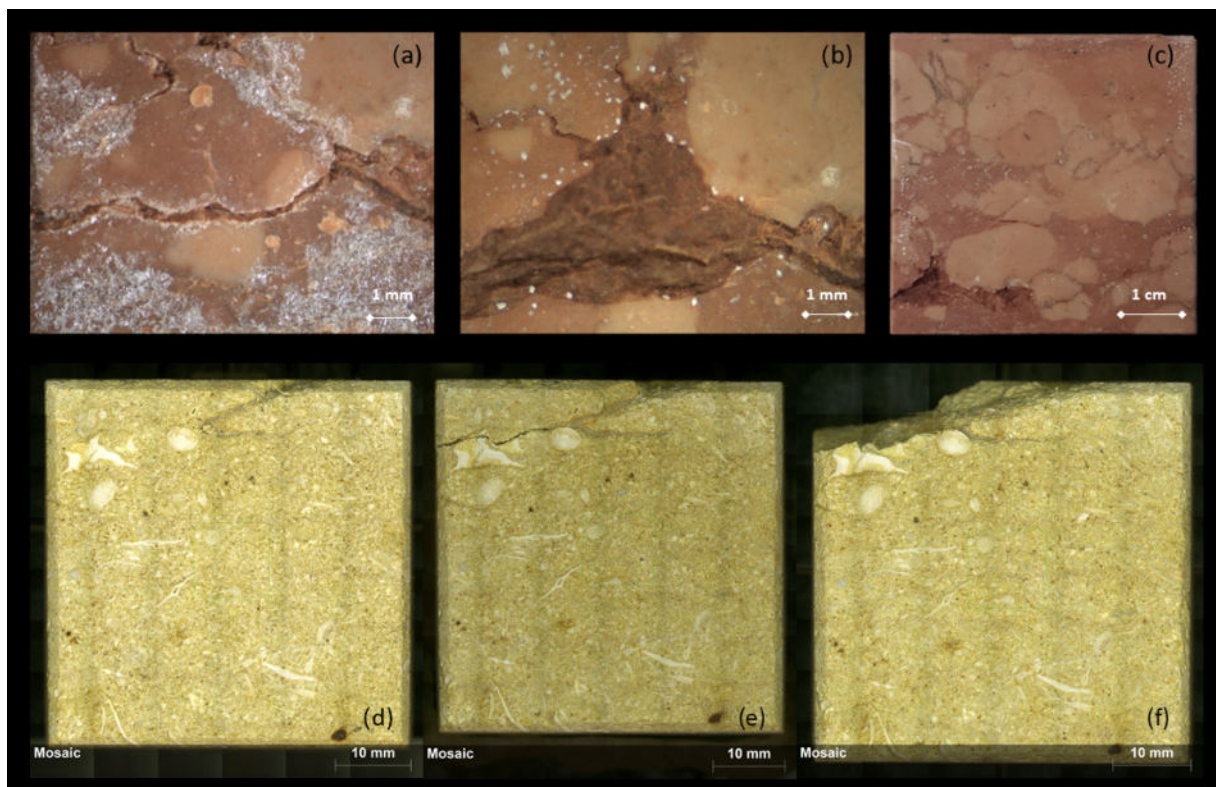
Figure 10. Examples of physical degradation. Loss of material due to the crystallization of salts in *Ammonitico Rosso* from Verona specimen exposed at *Palazzo Malipiero* (P2): comparison between a detail of specimen at t_4 (**a**) and t_5 (**b**) and the image of the entire specimen at t_5 (**c**). Detachment of material among a structural discontinuity in *Vicenza Soft Stone* specimen exposed at *Palazzo Malipiero* (P2): comparison between the specimen at t_6 (**d**) t_7 (**e**) and t_8 (**f**).

G.   Decohesion

The exposure time was sufficient to determine a significant physical deterioration of most of the specimens in P2. It corresponds to a loss of compactness measured by verifying the ultrasonic speed [30,31]. This physical decay is explained by the position of these samples, since at the upper level they suffer more wet and dry cycles and, consequently, salt crystallization. The action of the salts and the thermal changes lead to the formation of inner micro-cracks, as demonstrated by ultrasonic analysis. Particularly significant is the trend of the ultrasonic speed curve recorded for *White Carrara Marble* specimens in all the sites, as shown in Figures 8 and 11. Due to the holocrystalline mosaic microstructure of the marble and the well-known thermal anisotropy of calcite (the main constituent of the marble), when it is subjected to thermal shock, thermoclastism undergoes with consequent inter-crystalline decohesion of the calcite grains (baked marble).
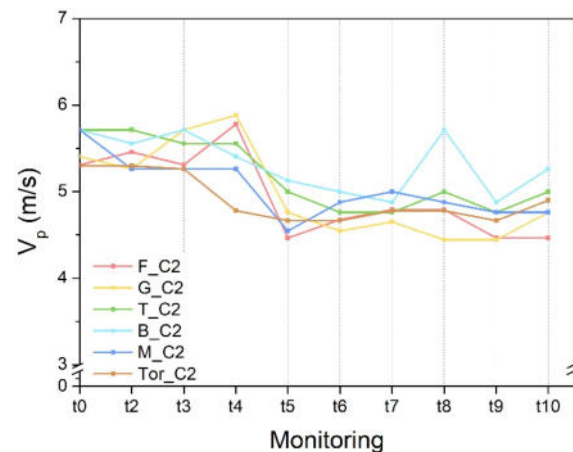
Figure 11. Ultrasonic speed variation measured in *White Carrara Marble* specimens placed in P2 at *Palazzo Badoer* (B), *Ca' Foscari* (F), *San Giobbe* campus (G), *Palazzo Malipiero* (M), *Torcello* island (Tor) and *Ca'Tron* (T).

H. Biodeterioration

The biological deterioration sticked out some lithotypes in different sites. The spread of spores in the atmosphere is a natural and common phenomenon as well as the tendency of spores to settle on surfaces. However, only favourable microclimatic conditions and suitable substrates allow the development and growth of biodeteriogens, such as algae, cyanobacteria and micromycetes [32–34]. In the case of the selected sites, colonisations of different organisms were revealed exclusively at *Palazzo Badoer* and *Palazzo Malipiero*. In the case of *Palazzo Badoer* (especially for the specimens in P1), the presence of fungal hyphae was recognised thanks to the classic chain structure that characterizes the micromycetes growth, as demonstrated by freshly prepared slides (Figure 12) [15]. The sheltered location, the low altimetry of this site and the high tide phenomena in November and December 2019 allowed the growth of these microorganisms. On the other hand, all the specimens in P1 at *Palazzo Malipiero* showed green algae and cyanobacteria—as confirmed by the study of freshly prepared slides (Figure 13) [15]—due to the continuous exposure to wave motion and floods caused by the marine traffic and high tides, respectively. Among all lithotypes, *Vicenza Soft Stone* shows the greatest biological and algal surface colonization (Figure 14), since its higher porosity [32–34]. A negligible development of green algae and cyanobacteria was observed on *White Carrara Marble* and *Istrian Stone*, in the specimens in P1 at both *Ca' Foscari* and *San Giobbe* sites, determined by the effects of the continuous wave motion. Crusty lichens developed only on *White Carrara Marble* in *Torcello* Island, although in a low quantity, as shown in Figure 15.
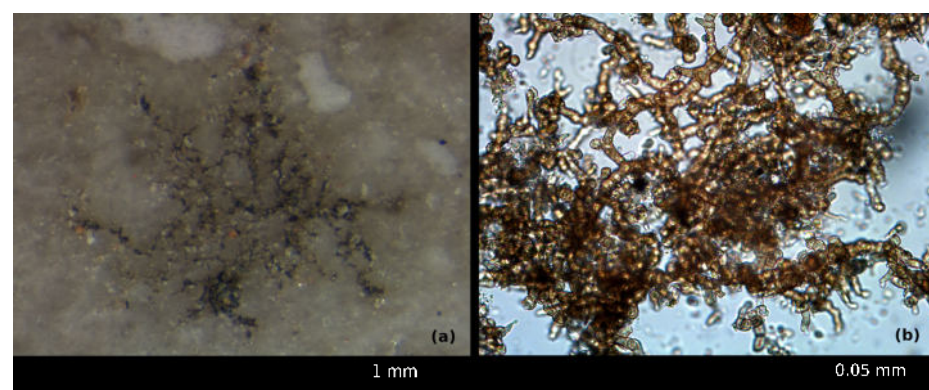

Figure 12. Stereograph (**a**) and micrograph (**b**) of fungi observed on the exposed surface of *Aurisina Fiorita Stone* placed at *Palazzo Badoer* (P1). Reflected light.
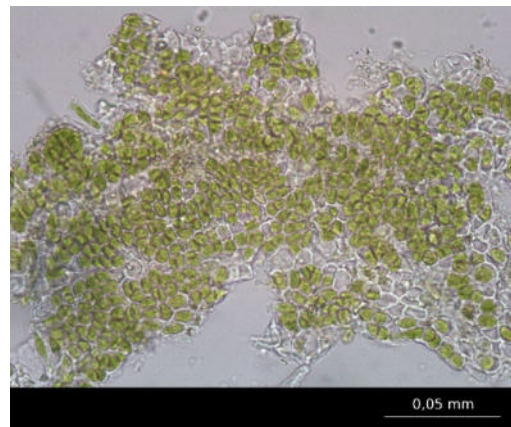
Figure 13. Fragment of green algae sampled from *Vicenza Soft Stone* specimen exposed at *Palazzo Malipiero* (P1).
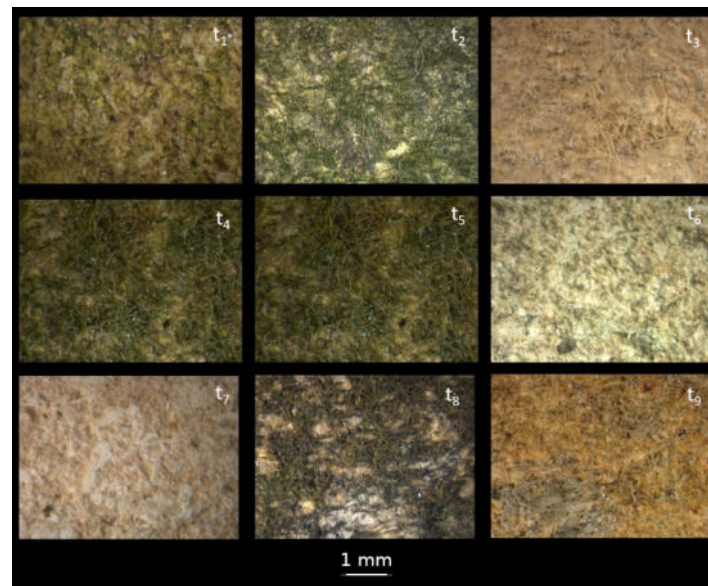

Figure 14. Stereographs of *Vicenza Soft Stone* specimen at *Palazzo Malipiero* (P2) from September 2019 to February 2022 (from t_1 to t_9): evolution of the growth of green algae.
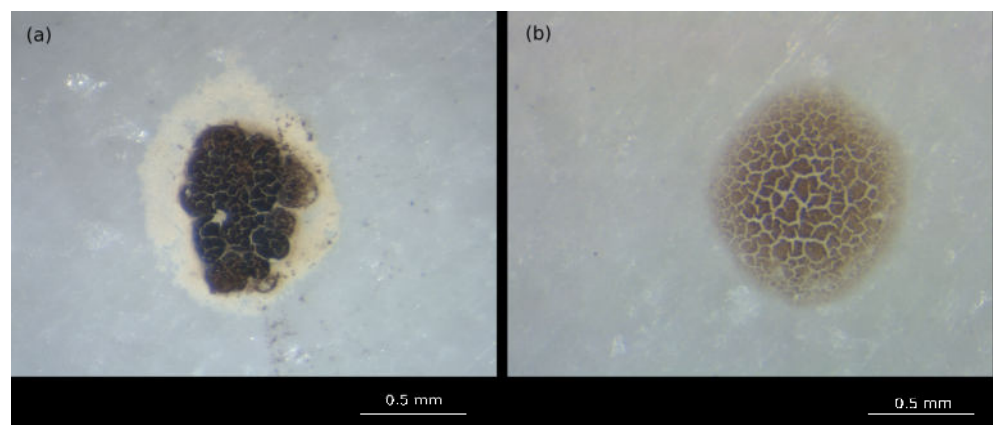

Figure 15. Stereographs of reddish crusty lichen (**a**) and black crusted lichens (**b**) developed on *White Carrara Marble* specimens in P2 and P1 exposed on *Torcello* Island and observed during the second monitoring (Tor-C1_t_2). Long side image 2.5 mm.

3.2. Decay Prediction Models for the Studied Lithotypes

Within the intervention and conservation programme of "Venezia 2021" project, in order to develop strategies to protect and safeguard the historical and architectural heritage of Venice, a model forecast and a *Stone Deterioration and Intervention index* (*SDIi*) were developed.

I.   Loss of compactness prediction

From the data collected during the outdoor exposure, an algorithm was developed with the programming and numeric computing platform MATLAB. This algorithm provides a forecast on the trend of the propagation speed of the ultrasonic waves according to the lithology, the location site and the two considered altimetric positions in each pilot site.

The provided forecast is based on the ultrasonic speed data collected between September 2019 and February 2022, related to a series of meteorological factors that can influence the variation of this parameter. Specifically, for each monitoring were considered the amount of total precipitation, the tide level (Figure 16), the daily average of temperature, the daily average of relative humidity and the daily total solar radiation in the period between a specific monitoring and the previous one. For the meteorological factors, data from the ARPAV databases and the forecast centre and tide report of Venice Municipality (*Centro Previsioni e Segnalazioni Maree*) were used. Each of these parameters was related to the variation (%) of ultrasound speed compared to the previous period. In this way, it was possible to obtain a predicted range of the ultrasonic speed for future monitoring. The values of the meteorological factors between the last monitoring and the future one, which are assumed to be performed on the forecast, can be obtained from the above (or estimated based on previous) years. Potentially, this could be protracted, thus offering an estimation on a more extended time scale than expected. It is therefore evident that the longer the monitoring carried out, or rather the quantity of data collected, and more reliable the model is, so that virtually a generic model could be developed.
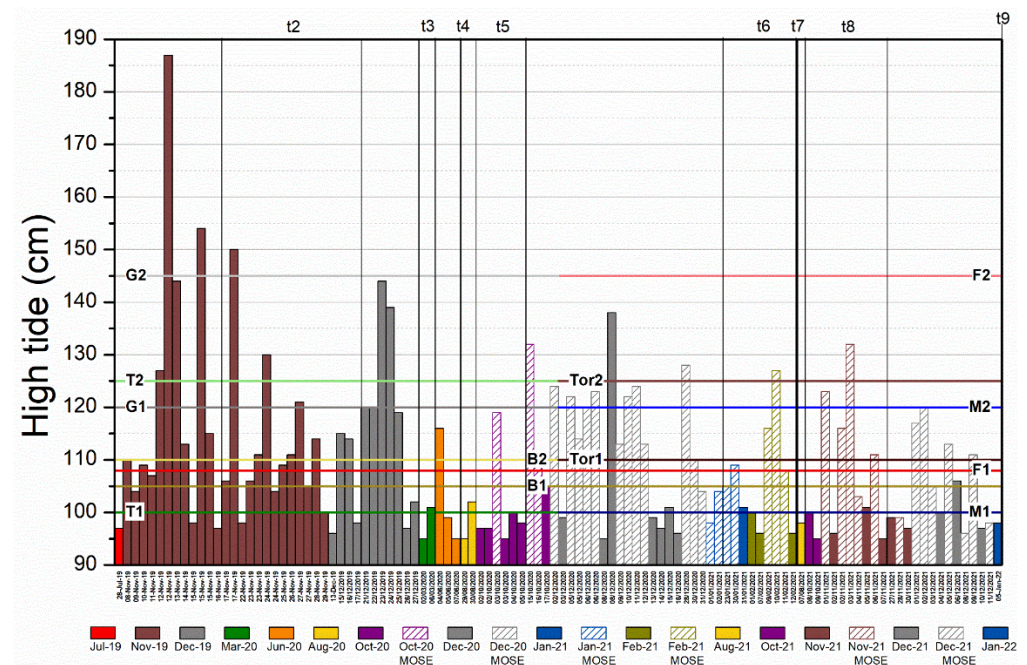

Figure 16. High tide occurred from July 2019 and January 2022 and correspondent altimetry of each sample: B1 (*Palazzo Badoer*, P1—dark yellow line); B2 (*Palazzo Badoer*, P2—light yellow line); T1 (*Ca' Tron*, P1—dark green line); T2 (*Ca' Tron*, P2—light green line); G1 (*San Giobbe* campus, P1—dark grey line); G2 (*San Giobbe* campus, P2—light grey line); F1 (*Ca' Foscari*, P1—dark red line); F2 (*Ca' Foscari*, P2—light red line); M1 (*Palazzo Malipiero*, P1—dark blue line); M2 (*Palazzo Malipiero*, P2—light blue line); Tor1 (*Torcello* island, P1—dark brown line) and Tor2 (*Torcello* Island, P2—light brown line).

The ultrasonic wave propagation speed range simulated for the tenth monitoring is revealed to be reliable with respect to the experimental measurements collected, so it is possible to conclude that the results obtained using the forecast model are to be considered at least promising. Figure 17 shows an example of output provided by the forecast model for the *Vicenza Soft Stone*. Each graph represents a sample for which a probable ultrasonic speed range has been calculated, represented by the red vertical bar, on which the actual experimental measurement performed during the last monitoring was then plotted.
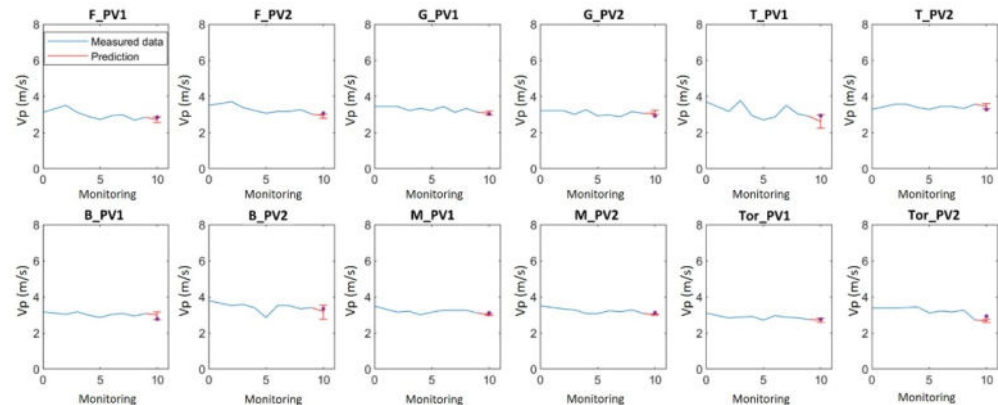

Figure 17. Forecast of the ultrasonic speed variation of *Vicenza Soft Stone* specimens and plot of the actual measured data.

II. Stone Deterioration and Intervention index

The same data collected from the monitoring sessions were used to develop and propose a straightforward deterioration and intervention index. This index is not related to a specific lithotype, but to the variation of two properties typically considered in the characterization of stone monumental surfaces and easily measurable in situ, through portable instruments and without destructive analyses, such as the propagation speed of ultrasonic waves and colour variation. This parameter has been defined as *Stone Deterioration and Intervention index* (*SDIi*):

$$SDIi = \left(\frac{v_P}{v_{P_0}} \right)^{(v_{P_0} - v_P) \cdot \sqrt{\Delta E^*}}$$

where v_{P_0} is the propagation speed of the ultrasonic waves in the considered specimen at t_0, v_P is the propagation speed of the ultrasonic waves of the specimen at a later time, ΔE^* is the chromatic variation with respect to the original colour in space $CIEL^*a^*b$.

Algebraically, *SDIi* can assume values between 1 (sample not deteriorated and qualitatively unchanged) and 0 (sample deteriorated and qualitatively altered). It represents an approximate but sensible, easy and rapid estimation of the deterioration that has occurred and an expeditious assessment of the need to intervene or not on it with further observations/analyses more detailed or/and conservative treatments or/and restoration operations, depending on the specific case and the lithotype in question. This is evident if we consider that significant colour variations may also be due to the formation of biodeteriogens and efflorescence on the surface in the Venetian context.

The *SDIi* applied to the exposed samples, at the end of the exposure period (June 2019–February 2022), provided the results reported in Table 5.

Table 5. *SDIi* index applied to the exposed samples at the end of the exposure period considered (June 2019–February 2022).

Lithotype	Position	*Palazzo Badoer*	*Ca' Tron*	*San Giobbe* Campus	*Ca' Foscari*	*Palazzo Malipiero*	*Torcello* Island
White Carrara Marble	1.	0.46	0.82	0.23	0.63	0.39	0.83
	2.	0.93	0.81	0.80	0.64	0.75	0.90
Istrian Stone	1.	0.99	0.94	0.94	0.99	0.89	1.00
	2.	0.99	0.98	0.99	0.96	0.96	1.00
Aurisina Fiorita Stone	1.	0.85	0.80	0.83	0.99	0.99	0.99
	2.	0.94	0.98	0.99	0.99	0.76	0.99
Ammonitico Rosso from Verona	1.	0.99	0.97	0.97	0.99	0.99	1.00
	2.	0.94	0.89	0.98	0.99	0.96	0.98
Vicenza Soft Stone	1.	0.85	0.72	0.93	0.93	0.83	0.90
	2.	0.85	1.00	0.93	0.88	0.86	0.88

4. Conclusions

In light of the practical implications of the study's findings, it is evident that the deterioration patterns exhibited by Venetian historical building specimens after three years of exposure to natural aging are multifaceted. The key forms of deterioration identified include chromatic alterations, efflorescence and subflorescence, sulphation, surface concretions, loss of material, decohesion, and biodeterioration [35,36].

These findings underscore the intricate interplay between environmental forces and intrinsic stone properties, such as mineralogical and chemical composition, physical structure, texture, and porosity. Importantly, the unique characteristics of each lithology significantly influence the deterioration pattern, reflecting the diverse conditions of exposure within the respective sampling sites.

Furthermore, the study's results have significant implications for the preservation and conservation of Venetian cultural heritage. By elucidating the specific deterioration mechanisms affecting historical buildings, the research provides valuable insights for developing targeted intervention strategies. Preservation efforts can be tailored to address the identified forms of deterioration and mitigate their impact on architectural surfaces.

In summary, the study's findings contribute to a deeper understanding of the environmental challenges facing Venetian historical buildings and underscore the importance of proactive preservation measures. By addressing the complex interplay between environmental factors and intrinsic stone properties, the research lays the groundwork for effective preservation strategies tailored to the unique characteristics of Venetian cultural heritage.

To enhance the reliability of estimating the vulnerability of the selected lithology and to establish methodologies for intervention and conservation plans, the results derived from experimental measurements were utilized to develop a forecast model based on climatic data from the exposure period. The simulated ultrasonic wave propagation speed, generated using the developed algorithm, demonstrated robustness in comparison to the experimental measurements collected. The outcomes generated by the forecasting model, which are potentially open and implementable, play a crucial role in determining a feasible intervention threshold. The *Index of Deterioration and Intervention for Stone Materials* (*SDIi*) serves as a valuable tool in estimating deterioration and assessing the necessity for additional analyses and intervention through conservative and targeted actions. In this context, the conservator-restorer can leverage this parameter, informed by the routine monitoring analysis of the stone material's conservation status, to determine the optimal timing for artifact preservation efforts. Moreover, the *SDIi* index, albeit not fully comprehensive, benefits from the fact that the data on which it is based can be obtained through portable instruments and non-destructive analyses, which can be routinely applied

directly by the technical offices of the institutional bodies responsible for managing the architectural heritage.

The results provided by the *SDIi* can be correlated with what was observed on the specimens exposed to natural ageing. On the contrary, in some cases, for example for *Vicenza Soft Stone* and *Ammonitico Rosso from Verona* specimens, it is evident that the specimens, exposed to atmospheric agents and the Venetian lagoon environment, are characterized by an overestimated *SDIi*. This is mainly due to the difficulty in accurately assessing the influence of the quantity of salts (especially within the limits) in the sample on the measurement of the ultrasound propagation speed. During the monitoring of naturally aged samples, it happened on several occasions that the measured ultrasound propagation speed was greater than the ultrasonic speed at the initial time, a phenomenon that was correlated to the influence of salts deposition inside the sample (that corresponds to a significant, even if partial, occlusion of the pores).

In conclusion, we can speculate that the future of cultural heritage conservation may be guided by an increasingly integrated and technologically advanced approach. Potential future directions could include the development of real-time monitoring systems for continuous surveillance of the conservation status of stone materials exposed to atmospheric agents. Furthermore, the use of artificial intelligence techniques could contribute to improving the prediction of deterioration patterns and optimizing conservative intervention strategies. The implementation of interdisciplinary approaches, involving experts in environmental sciences, engineering, and restoration, could enable the development of innovative and sustainable solutions for cultural heritage conservation.

References

1. Sesana, E.; Gagnon, A.S.; Ciantelli, C.; Cassar, J.; Hughes, J.J. Climate change impacts on cultural heritage: A literature review. *WIREs Clim Change* **2021**, *12*, e710. [CrossRef]
2. Cavaleri, L. The oceanographic tower Acqua Alta-activity and prediction of sea states at Venice. *Coast. Eng.* **2000**, *39*, 29–70. [CrossRef]
3. Comerlati, A. Saving Venice by seawater. *J. Geophys. Res.* **2004**, *109*, 1–14. [CrossRef]
4. Camuffo, D. Analysis of the Sea Surges at Venice from A.D. 782 to 1990. *Theor. Appl. Climatol.* **1993**, *47*, 1–14. [CrossRef]

5.   Gatto, P.; Carbognin, L. The Lagoon of Venice: Natural environmental trend and man-induced modification. *Hydrol. Sci. Bull.* **1981**, *26*, 379–391. [CrossRef]

6.   Trincardi, F.; Barbanti, A.; Bastianini, M.; Benetazzo, A.; Cavaleri, L.; Chiggiato, J.; Papa, A.; Pomaro, A.; Sclavo, M.; Tosi, L.; et al. The 1966 Flooding of Venice: What Time Taught Us for the Future. *Oceanography* **2016**, *29*, 178–186. [CrossRef]

7.   Antonelli, F.; Lazzarini, L.; Cancelliere, S.; Tesser, E. Study of the deterioration products, gilding, and polychromy of the stones of the Scuola Grande di San Marco's façade in Venice. *Stud. Conserv.* **2016**, *61*, 74–85. [CrossRef]

8.   Salvini, S.; Coletti, C.; Maritan, L.; Massironi, M.; Pieropan, A.; Spiess, R.; Mazzoli, C. Petrographic characteriztion and durability of carbonate stones used in UNESCO World Heritage Sites in northeastern Italy. *Environ. Earth Sci.* **2023**, *82*, 49. [CrossRef]

9.   Antonelli, F. The stones (of Venice) tell stories: How to read them | Le pietre (di Venezia) raccontano: Come leggerle. *Vesper* **2019**, *1*, 196–203.

10. Zaccariello, G.; Tesser, E.; Piovesan, R.; Antonelli, F. Evaluating the Effects of High Tide on Venetian Stone Buildings: A Multi-Analytical Approach. In *Proceedings of TC4 MetroArchaeo 2020 (ONLINE)-IMEKO TC4 International Conference on Metrology for Archaeology and Cultural Heritage*; International Measurement Confederation (IMEKO): Budapest, Hungary, 2020; pp. 27–31.

11. *EN 15886:2010*; Conservation of Cultural Property-Test Methods-Colour Measurement of Surfaces. European Standards: Plzen, Czech Republic, 2010.

12. Tesser, E.; Antonelli, F. Evaluation of silicone based products used in the past as today for the consolidation of Venetian monumental stone surfaces. *Mediterr. Archaeol. Archaeom.* **2018**, *18*, 159–170. [CrossRef]

13. Mokrzycki, W.S.; Tatol, M. Colour difference ΔE-A survey. *Mach. Graph. Vis.* **2011**, *20*, 383–411.

14. Palazzi, S. *Colorimetria: La Scienza del Colore nell'arte e Nella Tecnica*; Nardini: Florence, Italy, 1995; ISBN 8840440402.

15. *UNI 10923:2001*; Cultural Heritage-Natural and Artificial Stones-Preparation of Biological Specimens for the Observation by Light Microscopy. Ente Nazionale Italiano di Unificazione (UNI): Milano, Italy, 2001.

16. *UNI EN 14579:2005*; Natural Stone Test Methods-Determination of Sound Speed Propagation. Ente Nazionale di Unificazione: Milano, Italy, 2005.

17. Berto, L.; Favaretto, T.; Saetta, A.; Antonelli, F.; Lazzarini, L. Assessment of seismic vulnerability of art objects: The Galleria dei Prigioni sculptures at the Accademia Gallery in Florence. *J. Cult. Herit.* **2012**, *13*, 7–21. [CrossRef]

18. Bergin, M.H.; Tripathi, S.N.; Devi, J.J.; Gupta, T.; Mckenzie, M.; Rana, K.S.; Shafer, M.M.; Villalobos, A.M.; Schauer, J.J. The discoloration of the Taj Mahal due to particulate carbon and dust deposition. *Environ. Sci. Technol.* **2015**, *49*, 808–812. [CrossRef] [PubMed]

19. Bams, V.; Dewaele, S. Staining of white marble. *Mater. Charact.* **2007**, *58*, 1052–1062. [CrossRef]

20. Granneman, S.J.C.; Lubelli, B.; van Hees, R.P.J. Mitigating salt damage in building materials by the use of crystallization modifiers–a review and outlook. *J. Cult. Herit.* **2019**, *40*, 183–194. [CrossRef]

21. Cardell, C.; Delalieux, F.; Roumpopoulos, K.; Moropoulou, A.; Auger, F.; Van Grieken, R. Salt-induced decay in calcareous stone monuments and buildings in a marine environment in SW France. *Constr. Build. Mater.* **2003**, *17*, 165–179. [CrossRef]

22. Kramar, S.; Urosevic, M.; Pristacz, H.; Mirtič, B. Assessment of limestone deterioration due to salt formation by micro-Raman spectroscopy: Application to architectural heritage. *J. Raman Spectrosc.* **2010**, *41*, 1441–1448. [CrossRef]

23. La Russa, M.F.; Comite, V.; Aly, N.; Barca, D.; Fermo, P.; Rovella, N.; Antonelli, F.; Tesser, E.; Aquino, M.; Ruffolo, S.A. Black crusts on Venetian built heritage, investigation on the impact of pollution sources on their composition. *Eur. Phys. J. Plus* **2018**, *133*, 370. [CrossRef]

24. Tesser, E.; Conventi, A.; Majerle, F. Characterization of Barium Hydroxide Used as Consolidating Agent for Monumental Surfaces in Venice. *Heritage* **2022**, *5*, 3280–3297. [CrossRef

25. Zaccariello, G.; Tesser, E.; Piovesan, R.; Gasperuzzo, G.; Simionato, R.; Antonelli, F. Climate change and land subsidence in the frame of "Venezia 2021" project: The deterioration of architectural stone materials. In Proceedings of the TC4 MetroArchaeo 2022-IMEKO TC4 International Conference on Metrology for Archaeology and Cultural Heritage, Consenca, Italy, 19–21 September 2022; International Measurement Confederation (IMEKO): Budapest, Hungary, 2022; pp. 27–31.

26. Maravelaki-Kalaitzaki, P.; Biscontin, G. Origin, characteristics and morphology of weathering crusts on Istria stone in Venice. *Atmos. Environ.* **1999**, *33*, 1699–1709. [CrossRef]

27. Bortolaso, G.; Lazzarini, L.; Menegazzo Vitturi, L.; Rampazzo, G. The deterioration of "Rosso Ammonitico Veronese" nodular limestone: Comparison between a quarry and a Venetian monument. In Proceedings of the "Fifth International Congress on Deterioration and Conservation of Stone", Torun, Poland, 12–14 August 1988; pp. 97–109.

28. Antonelli, F.; Gentili, G.; Renzulli, A.; Amadori, M. Provenance of the ornamental stones used in the baroque church of S. Pietro in Valle (Fano, Central Italy) and commentary on their state of conservation. *J. Cult. Herit.* **2003**, *4*, 299–312. [CrossRef]

29. Cattaneo, A.; De Vecchi, G.P.; Menegazzo Pitturi, L. Le pietre tenere dei Colli Berici. Atti e memorie dell'Accademia Patavina di Scienze, Lettere ed Arti, V.LXXXVIII (1975–1976), Parte II, Classe di Scienze Matematiche e Naturali. Soc. cooperativa tip. Padua, Italy. 1976, pp. 69–100. Available online: https://www.culturaveneto.it/it/beni-culturali/libri/le-pietre-tenere-dei-colli-berici (accessed on 20 May 2024).

30. Molina, E.; Cultrone, G.; Sebastián, E.; Alonso, F.J. Evaluation of stone durability using a combination of ultrasound, mechanical and accelerated aging tests. *J. Geophys. Eng.* **2013**, *10*, 035003. [CrossRef]

31. Rodrigues, J.D.; Costa, D. The conservation of granite in Évora Cathedral. From laboratory to practice. In Proceedings of the Int. Symp. "Stone Consolidation in Cultural Heritage. Research and Practice", Lisbon, Portugal, 6–7 May 2008; Delgado Rodrigues, J., Mimoso, J.M., Eds.; LNEC: Lisboa, Portugal; pp. 101–110.

32. Caneva, G. Complessità degli aspetti gestionali delle comunità vegetali in aree archeologiche: Il caso del Palatino. In Proceedings of the 40° Congresso Della Società Italiana Di Fitosociologia, Rome, Italy, 19–21 February 2004; pp. 9–11.

33. Caneva, G.; Nugari, P.; Salvadori, O. *La biologia vegetale per i beni Culturali*; Nardini Editore: Florence, Italy, 2007; ISBN 9788840441535.

34. Tommaselli, L.; Lamenti, G.; Tiano, P. Relationships between stone-dwelling cyanobacteria and damage. In Proceedings of the 2nd International Congress, Science and Technology for the Safeguard of Cultural Heritage in the Mediterranean Basin, Paris, France, 5–9 June 1999; pp. 841–842.

35. ICOMOS; ISCS. *ICOMOS-ISCS: Illustrated Glossary on Stone Deterioration Patterns*; Vergès-Belmin, V., Ed.; XV; ICOMOS: Paris, France, 2008.

36. Piovesan, R.; Tesser, E.; Maritan, L.; Zaccariello, G.; Mazzoli, C.; Antonelli, F. Mapping of stones and their deterioration forms: The Clock Tower, Venice (Italy). *Herit. Sci.* **2023**, *11*, 108. [CrossRef]